J Appl Electrochem (2014) 44:1135–1143
DOI 10.1007/s10800-014-0739-2

RESEARCH ARTICLE

Cu^{2+}, Fe^{2+} and Fe^{3+} analysis of bioleaching solutions using chronoamperometry and BDD electrode

Mikko Vepsäläinen · Miao Chen · Yi Yang · Rachel Brokenshire · Tim Muster

Received: 23 April 2014 / Accepted: 18 August 2014 / Published online: 24 August 2014

Abstract In this work, a boron-doped diamond (BDD) electrode was evaluated for the electroanalytical determination of millimolar concentrations of Cu^{2+}, Fe^{2+} and Fe^{3+} using chronoamperometry. The interfering role that each ion plays on the quantitative determination of other metal ion concentrations was also assessed. No interference from other metal ions was observed when Fe^{3+} and Fe^{2+} were analysed. By contrast, reduction of Fe^{3+} took place at the same potential where $[Cu^{2+}]$ was measured causing a minor interference to the Cu^{2+} signal. A multiple linear regression (MLR) calibration model was made for each analyte using real bioleaching samples, which demonstrated high coefficients of determination and adequate standard errors. The methods developed were used to monitor bioleaching of chalcopyrite for 4 months. The electroanalytical methods are particularly well-suited for analysing Cu^{2+}, Fe^{3+} and Fe^{2+} concentration in acidic mine drainage (AMD) and bioleaching environments.

Keywords Acid mine drainage · Bioleaching · Boron-doped diamond · Chronoamperometry

1 Introduction

Acid mine drainage (AMD) is a serious environmental problem which causes long-term environmental degradation. AMD is toxic to aqueous species in the receiving watercourses due to its low pH and ability to solubilise transition metals, such as iron, aluminium, manganese, copper and cadmium [1–3]. In their soluble forms, some of these metals, such as copper, have acute toxicity, while their precipitation on a sediment surface also inhibits the reproduction of benthic organisms [4, 5]. The major cause of AMD is the oxidation of pyrite (FeS_2) and other sulphide minerals, a process which releases protons. Ferric ions are the main oxidant which drives this reaction and the ferrous ion byproducts are re-oxidised to ferric species through chemical or microbiological reactions. If the pH is below four, biotic oxidation is the main mechanism [6]. Examples of reactions releasing metal ions are the oxidation of pyrite (Eq. 1) and chalcopyrite (Eq. 2).

$$2FeS_2 + 7O_2 + 2H_2O \rightarrow 2Fe^{2+} + 4SO_4^{2-} + 4H^+ \quad (1)$$

$$CuFeS_2 + 4Fe^{3+} \rightarrow 5Fe^{2+} + Cu^{2+} + 2S^0 \quad (2)$$

The microbiological processes of AMD are utilised industrially as bioleaching processes, such as heap bioleaching of copper ores, where acidophilic iron- and sulphur-oxidising bacteria assist in the extraction of metals from mineral sulphides [7]. Ferric ions are recycled according to Eq. 3 and sulphur is oxidised to sulphate according to Eq. 4.

$$4Fe^{2+} + 4H^+ + O_2 \rightarrow 4Fe^{3+} + 2H_2O \quad (3)$$

$$2S^0 + 3O_2 + 2H_2O \rightarrow 2H_2SO_4 \quad (4)$$

Both AMD and bioleaching effluents are acidic; with AMD typically pH 2–3, whilst the pH of chalcopyrite bioleaching is kept in the range between 1 and 2 to enhance leaching rates and reduce jarosite formation [7, 8]. During the bioleaching of chalcopyrite the concentration of copper and iron species can reach 100 mM or even higher [9–11] and optimising this process requires analysis and control of the Cu^{2+}, Fe^{3+} and Fe^{2+} ions that are released.

M. Vepsäläinen (✉) · M. Chen · Y. Yang · R. Brokenshire
CSIRO Mineral Resources Flagship, Box 312, Clayton South, Melbourne, VIC 3169, Australia
e-mail: mikko.vepsalainen@csiro.au

T. Muster
CSIRO Land and Water Flagship, Private Bag 33, Clayton South, Melbourne, VIC 3169, Australia

There is a wide variety of analytical methods that are suitable for measuring copper and iron concentrations in AMD and bioleaching process solutions; for example inductively coupled plasma optical emission spectrometry (ICP-OES), atomic absorption spectroscopy (AAS), spectrophotometry and titration. However, most of these methods are destructive and analysis is performed off-site. Electroanalytical techniques have several benefits compared to these alternatives: quick and cheap analysis, non-destructive and easier conversion to an on-line method. Ion-selective electrodes are commercially available for copper but they suffer from the influence of interfering ions, especially Fe^{3+} in the case of AMD and bioleaching [12, 13].

Voltammetry has been used to measure copper concentrations in AMD [14] and also for the determination of trace amounts of copper in honey [15]. The most commonly used working electrodes for voltammetry are hanging mercury drop electrode (HDME) and mercury film electrodes but the toxicity of mercury and the requirement for surface renewal are drawbacks of these materials. Boron doped diamond (BDD) is a relatively new electrode material which has good mechanical strength, low capacitive background, good conductivity and a wide potential window with practically no anodic corrosion [16–19]. BDD is therefore replacing mercury electrodes in many electro-analytical applications. A comparison of BDD with Hg for the measurement of metal ion concentrations in contaminated water samples by anodic stripping voltammetry found that BDD had similar properties to Hg in this application [20]. Stripping voltammetry using BDD enables concentrations down to nanomolar to be measured in favourable conditions [21, 22]. Simultaneous detection of multiple cations is possible but there may be additional interferences, such as formation of lead-copper species when copper and lead cations are present in the solution [23].

In this work, the application of a BDD electrode for the electroanalytical determination of millimolar concentrations of Cu^{2+}, Fe^{2+} and Fe^{3+} was evaluated using chronoamperometry. The interfering role that each ion plays in the determination of the others was also assessed. A multiple linear regression (MLR) calibration model was made for Cu^{2+} and Fe^{3+} which also accounted for the effects of major interference. MLR analysis is a simple statistical method where the relationship of several independent predictor variables and a dependent variable is described by a linear regression model.

2 Experimental

2.1 Electrochemical measurements

Standard solutions were prepared using $Fe_2(SO_4)_3{\cdot}xH_2O$, $Fe_2SO_4{\cdot}7H_2O$ (Sigma-Aldrich) and $CuSO_4{\cdot}5H_2O$ (BDH Chemicals) analytical reagent grade chemicals. Concentrations of solutions were verified with ICP-OES (Agilent 730) due to the uncertainty in calculated concentration when water of crystallisation is present. The sample pH was adjusted using H_2SO_4 and NaOH solutions and measured using SevenMulti pH meter (Mettler Toledo) with an InLab Expert pH electrode.

Table 1 Parameters of the chronoamperometric (CA) measurements

Parameters	Cu^{2+}	Fe^{3+}	Fe^{2+}
Concentration range (mM)	0.01–100	0.007–73	0.01–105
Potential (mV) versus Ag/AgCl (1 M)	−500 (dep) and 200 (oxid)	100	1,050
Total time of CA (s)	5 (dep) and 50 (oxid)	10	10

A conventional three-electrode system was used in the studies. The rod-shaped BDD electrode (Neocoat SA, area 18.9 mm^2, doping level 800 ppm, microcrystalline) was cleaned before every measurement by cycling the applied potential between 2,000 mV and −1,000 mV 15 times at 300 mV/s in a well-stirred solution of H_2SO_4 (pH 2). The electrode was washed with milliQ water between measurements and before and after the electrochemical cleaning procedures. A platinum sheet was used as counter electrode and the reference was provided by a Ag|AgCl (1 M KCl) electrode from CH Instruments Inc. All potentials are reported with respect to this reference electrode. The solution conductivities were high because the pH was low so no supporting electrolyte was added. Measurements were carried out at room temperature using a computer controlled CHI 901A potentiostat (CH Instruments Inc) operating in the three-electrode mode. Cyclic voltammograms were recorded in the range of −1000 to 2,000 mV at the scan rate of 50 mV s^{-1}. Scans were initiated from 0 mV to the anodic direction. Calibration curves for Cu^{2+}, Fe^{3+} and Fe^{2+} were constructed using the chronoamperometric technique (Table 1). A single potential was used for Fe^{3+} and Fe^{2+} analyses whereas both reducing and oxidising potentials were used for Cu^{2+} analysis. The initial reducing potential deposited copper metal onto the electrode surface and the subsequent oxidising potential removed it.

2.2 Multiple linear regression calibration and monitoring of bioleaching

In order to calibrate the electrochemical sensor and verify its operation in real solutions, batch bioleaching experiments were conducted using three minerals; chalcopyrite, pyrite and low grade chalcopyrite. Chemical analysis of chalcopyrite and pyrite minerals is reported in a previous

paper [24]. These minerals represent the following bioleaching conditions; high copper and iron concentrations (chalcopyrite), low copper and high iron concentrations (pyrite) and low iron and copper concentrations (low grade chalcopyrite).

Acidithiobacillus ferrooxidans was used as bioleaching bacteria throughout the experiments. The bacterial strain has been adapted to chalcopyrite in CSIRO laboratories over a period of more than 2 years. The bacteria was cultured with the minerals in an orbital incubator (130 rpm, 30 °C) in 9 K environment containing 3.0 g L^{-1} $(NH_4)_2SO_4$, 0.5 g L^{-1} $MgSO_4{\cdot}7H_2O$, 0.5 g L^{-1} K_2HPO_4, 0.1 g L^{-1} KCl, 0.01 g L^{-1} $Ca(NO_3)_2$. After adjusting the pH of the 9 K solution to 1.8 using H_2SO_4, 150 mL was added to conical flasks containing 1.5 g of mineral. The study included three replicates per mineral. Evaporation losses were compensated with milliQ water.

Chemometric methods have previously been employed to analyse electrochemical data such as overlapping voltammograms [25–27]. In this study, the concentration of copper and iron was measured with ICP-OES (Agilent 730) and MLR calibration of the electrochemical sensor used these analytical results as the basis. The MLR calibration models constructed for $[Cu^{2+}]$ and $[Fe^{3+}]$ included the reduction current densities for Cu^{2+} and Fe^{3+} and the pH. The concentration of Fe^{2+} was very low in all bioleaching tests (current density below 0.03 mA cm^{-2}) and therefore $[Fe^{2+}]$ calibration was not performed when using bioleaching samples. Regression terms incorporated into the regression models were selected on the basis of their statistical significance test (p value <0.01).

3 Results and discussion

3.1 Cyclic voltammetry

The oxidation and reduction behaviour of individual Cu^{2+}, Fe^{3+} and Fe^{2+} ions on the BDD electrode during cyclic voltammetry are shown in Fig. 1. The cyclic voltammogram of Cu^{2+} (Fig. 1a) shows two peaks representing the reduction of Cu^{2+} to the metallic state at −550 mV and oxidation of metallic copper back to Cu^{2+} at 200 mV. On the first cycle, the oxidation peak was not seen since copper was not present on the surface. On BDD the reduction reaction commences at −200 mV and peak current occurs between −550 and −600 mV. According to background scans, hydrogen evolution begins at approximately −500 mV on the BDD electrode in pH 2 solution, so −500 mV was selected for the reductive analysis of Cu^{2+} to avoid hydrogen evolution interfering with the current signal. On the positive sweep the deposited copper was oxidised back to Cu^{2+} in the range of 0 to 500 mV

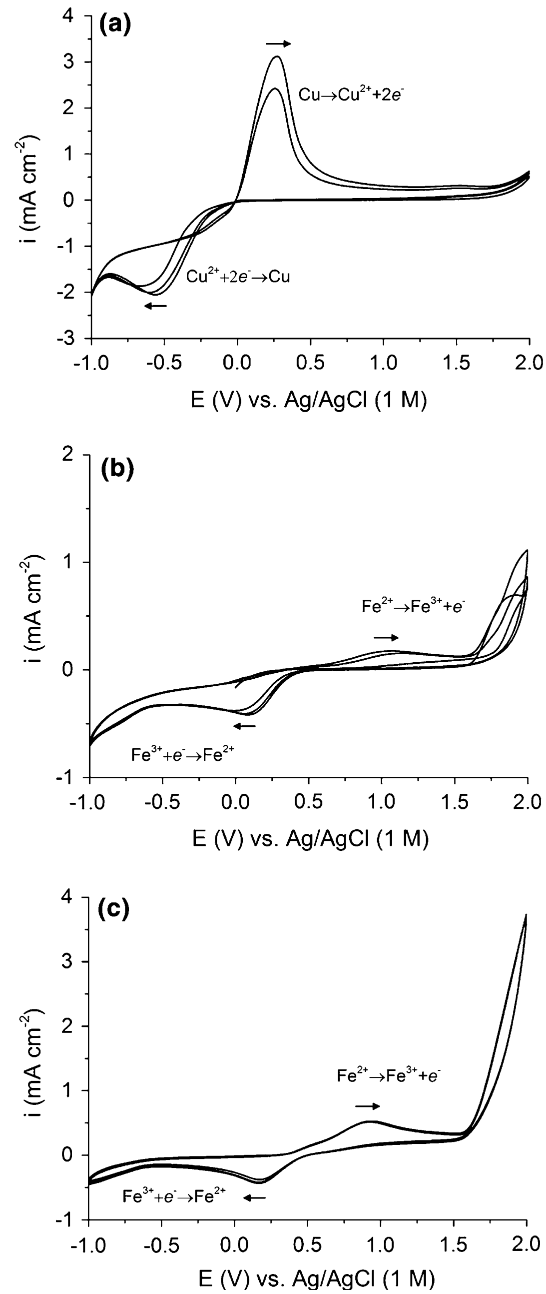

Fig. 1 Cyclic voltammogram of **a** $1.00{*}10^{-2}$ M Cu^{2+}, **b** $7.28{*}10^{-3}$ M Fe^{3+} and **c** $1.05{*}10^{-3}$ M Fe^{2+} in pH 2 solution recorded on a BDD electrode using a scan rate of 50 mV s^{-1}

(maximum at 200 mV), thus enabling a second analyses for Cu^{2+}. A complication can occur because sulphate, chloride and nitrate anions all have an effect on the nucleation of copper [28]. Cathodic reduction of Cu^{2+} occurs in two consecutive charge-transfer steps, through a soluble intermediate Cu^{+}. However, while Cu^{+} can be stabilised in chloride solutions, it is particularly unstable in sulphate solutions and no distinguishable peak for Cu^{+} is expected in the acidified sulphate electrolytes used in this study. The voltammograms in Fig. 1 have similar characteristics to

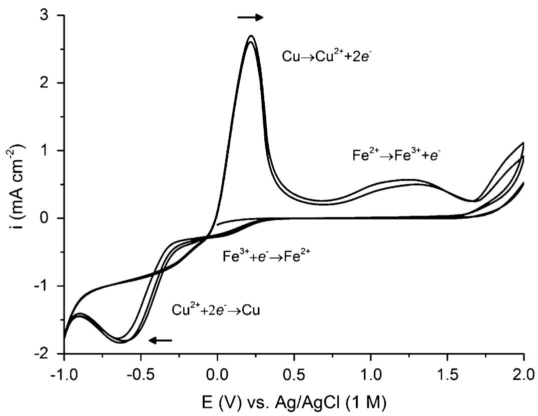

Fig. 2 Cyclic voltammogram of $1.00*10^{-3}$ M Cu^{2+} and $7.28*10^{-3}$ M Fe^{3+} in pH 2 solution recorded on a BDD electrode using a scan rate of 50 mV s^{-1}

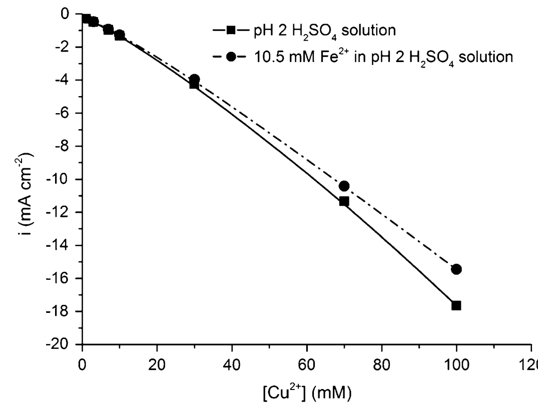

Fig. 3 Reductive current densities for chronoamperometric measurements 5 s after switching the applied potential to −500 mV versus Ag/AgCl (1 M) plotted against Cu^{2+} concentration with and without added Fe^{2+}

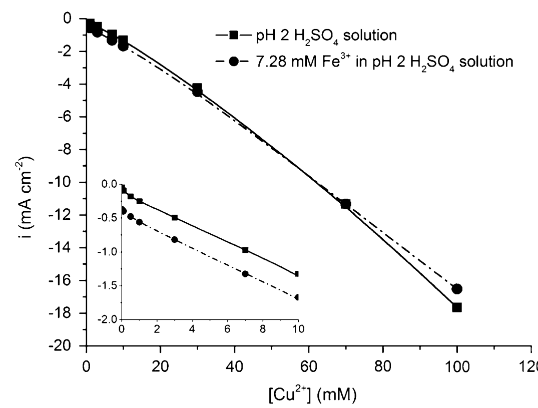

Fig. 4 Current densities for chronoamperometric measurement 5 s after switching the applied potential to −500 mV versus Ag/AgCl (1 M) plotted against Cu^{2+} concentration with and without added Fe^{3+}. The low concentration range is shown in the *inset*

those measured by Couto et al. in their copper electrodeposition studies [29]. Their results showed that surface termination of the BDD electrode has a strong influence on the copper deposition and dissolution processes. The BDD electrode used in this study was used without strong plasma or electrochemical treatments and therefore termination of the surface is unknown but is expected to be O-terminated.

Two peaks representing the reduction/oxidation reaction of Fe^{3+}/Fe^{2+} are clearly distinguishable in Fig. 1b and 1c. The peak potential of Fe^{3+} reduction is positioned at 1,050 V whereas the oxidation peak of Fe^{2+} is found at 0.1 V. These peaks have wide separation on the potential scale according to which the kinetics of the reduction/oxidation reaction are slow (i.e. irreversible or quasi-reversible electron transfer reaction).

To be able to measure the concentrations of both Cu^{2+} and Fe^{3+} ions in the same solution, their reduction peaks should be well separated or possible interference must minimised by other methods. According to the voltammogram (Fig. 2) where both Cu^{2+} and Fe^{3+} analytes were present in solution, the reduction peaks have adequate separation. However, high Fe^{3+} concentrations can cause some interference to the Cu^{2+} measurements, and therefore a thorough MLR calibration is required. Oxidation peaks for Cu and Fe^{2+} are well separated and no significant interference was observed in any of the chronoamperometric measurements.

3.2 Cu^{2+} detection

As described above, a reduction potential of −500 mV and oxidation potential of +200 mV were selected for the Cu^{2+} measurements based on the voltammetry. The deposition time at the reduction potential was kept short (5 s) and the following oxidation time was longer (50 s) to ensure the complete removal of deposited copper from the BDD surface. The calibration curve for Cu^{2+} was slightly curved in the range of 0.01–100 mM (Fig. 3) and the presence of 10.5 mM Fe^{2+} had an effect on the slope, especially at higher Cu^{2+} concentrations. The reason for this effect is described later. Current transients for the oxidation of plated copper were analysed but regression statistics and linearity were poor with the parameters used in this research.

Although the peaks for the reduction of Cu^{2+} and Fe^{3+}appeared well-separated, high concentrations of Fe^{3+} still interfered with Cu^{2+} measurements (Fig. 4). The effect of Fe^{3+} ions on Cu^{2+} reduction current was studied by adding 0.07–7.28 mM of Fe^{2+} to Cu^{2+} solutions. The presence of Fe^{3+} was found to shift the potential of the maximum reduction current negatively. Consequently the Fe^{3+} concentration was included in the MLR calibration model for Cu^{2+} analysis.

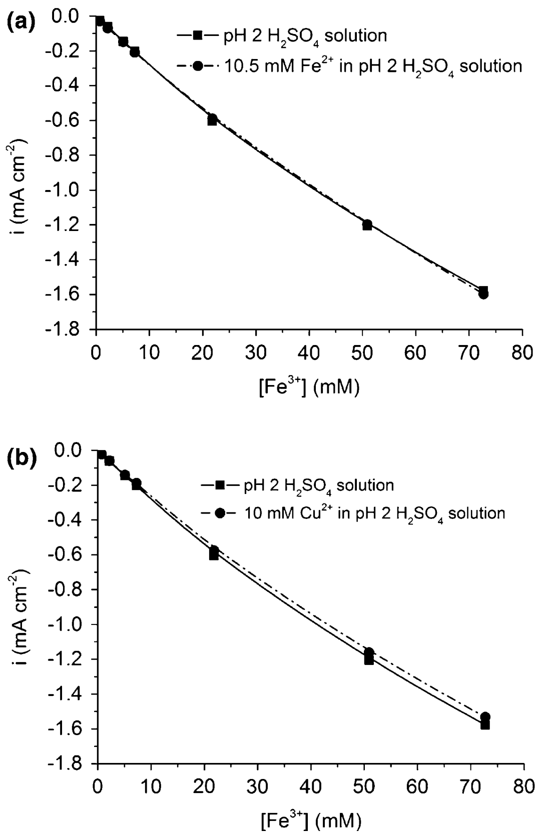

Fig. 5 Current densities for chronoamperometric measurements 10 s after switching the applied potential to +100 mV versus Ag/AgCl (1 M) plotted against Fe^{3+} concentration with and without **a** Fe^{2+} and **b** Cu^{2+} present in the solution

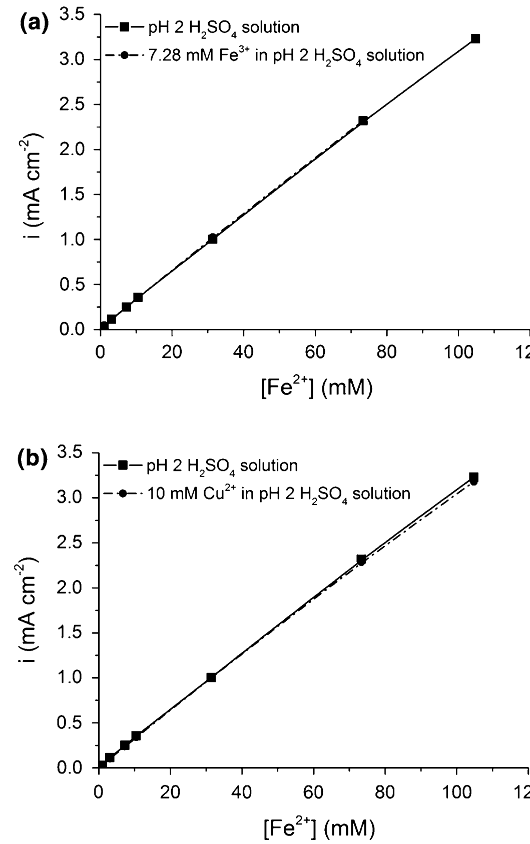

Fig. 6 Current densities for chronoamperometric measurements 10 s after switching the applied potential to +1,050 mV vs. Ag/AgCl (1 M) plotted versus Fe^{2+} concentration with and without **a** Fe^{3+} and **b** Cu^{2+} present in the solution

Both Fe^{3+} and Fe^{2+} affect electron transfer kinetics during copper electrodeposition and consequently, the slope of the chronoamperometric curve. The effect is particularly pronounced for Fe^{2+}. The Fe^{2+}/Fe^{3+} redox couple is utilised in the electronics industry to assist Cu plating in diffusion hindered locations [30] although the presence of Fe^{3+} ions is also known to lead to inefficiencies in Cu electrowinning [31]. These inefficiencies may result from slower electron exchange on the surface due to adsorbed Fe^{2+} and Fe^{3+} as well as from interferences arising from the concurrent reduction of Fe^{3+} to Fe^{2+} which will add to the overall measured current.

3.3 Fe^{3+} and Fe^{2+} detection

The reduction current for Fe^{3+} at +100 mV had an almost linear correlation with the Fe^{3+} concentration within the range studied: 1–75 mM (Fig. 5). As expected, Fe^{2+} did not affect the Fe^{3+} reduction current and while Cu^{2+} had a small effect on the slope of the curve, it did not produce any significant offsets. According to these results, Fe^{3+} can be measured without significant interferences.

The Fe^{2+} oxidation curve shows a linear relationship with the analyte concentration up to 105 mM (Fig. 6). The presence of Fe^{3+} and Cu^{2+} ions has no significant effect on the current signal and consequently these ions were not included in the MLR calibration model for Fe^{2+}.

3.4 Limit of detection (LOD), limit of quantitation (LOQ) and relative standard deviation (RSD)

The LOD, LOQ and RSD were calculated for the calibration curves (Figs. 3, 5 and 6). All these slopes were slightly curved and therefore second order polynomial functions were fitted to the data. LOD and LOQ were calculated according to Eq. 5 and Eq. 6.

$$\mathrm{LOD} = \frac{3\mathrm{SE}}{\mathrm{S}} \tag{5}$$

$$\mathrm{LOQ} = \frac{10\mathrm{SE}}{\mathrm{S}} \tag{6}$$

where SE is the standard error of the intercept and S is the slope of the regression. In this paper the linear term of the second order polynomial function is used as S. RSD was

Table 2 LOD, LOQ and RSD of the method for each analyte

	Cu^{2+}	Fe^{3+}	Fe^{2+}
LOD (mM)	0.40	0.34	0.37
LOQ (mM)	1.33	1.14	1.23
RSD (%)	0.82	1.03	1.16

evaluated by analysing 6 samples containing 10 mM of analyte in pH 2 H_2SO_4 solution. LOD of the metal ions was 0.3–0.4 mM, LOQ 1.14–1.33 mM and RSD 0.82–1.16 % (Table 2). Jin and Botte used a platinum rotating disk electrode to measure Fe^{2+} and Fe^{3+} [32]. The LOD of their method was 0.02 mM when rotation speed was 3,000 rpm, and the reproducibility was also superior compared to results shown in this paper. However, the method described in this paper is more suitable for on-site and on-line analysis due to simpler construction. The LOD, LOQ and RSD are suitable for analysing bioleaching solutions where the concentrations of metals is high.

3.5 Multiple linear regression analysis of the results

In total, 39 observations were incorporated into the MLR models for Cu^{2+} and Fe^{3+} analyses. Copper concentrations in the bioleaching samples, measured using ICP-OES, were between 0.01 and 1.70 g L^{-1} and iron concentrations between 0.01 and 2.92 g L^{-1}. The pH of the samples was not controlled during the bioleaching experiments and it varied from 1.43 to 2.57. High coefficients of determination were obtained for the MLR models (Fig. 7). Standard errors in the models for Cu^{2+} and Fe^{3+} were 0.047 g L^{-1} and 0.083 g L^{-1}, respectively. Possible sources of error are: temperature variations during the measurements and errors in electrochemical measurements and ICP-OES analyses. Nevertheless, according to the standard errors in the models, the analytical methods are suitable for monitoring bioleaching and AMD where the concentrations of both metals are relatively high.

The interaction term of current density of Cu^{2+} reduction and pH was the most important term in the Cu^{2+} model for explaining the variance (Table 3). The other statistically significant term was the current density of Fe^{3+} reduction. The presence of Fe^{3+} increases the reduction current density because the reduction potentials of Cu^{2+} and Fe^{3+} were slightly overlapping. Therefore, the coefficient of the reduction current density of Fe^{3+} in the Cu^{2+} model is positive. The reduction current densities of Cu^{2+} and Fe^{3+}, and interaction term of the reduction current density of Fe^{3+} and pH were statistically important terms of the Fe^{3+} calibration model (Table 4).

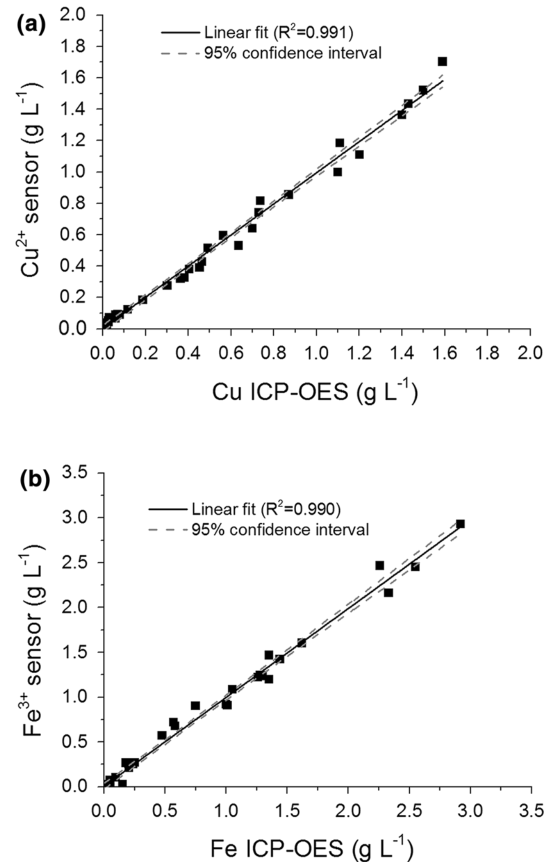

Fig. 7 **a** Copper and **b** iron concentration measured with ICP-OES and predicted by the MLR models

Bioleaching of chalcopyrite was monitored for 4 months with the electroanalytical methods developed (Fig. 8). The rate of bioleaching was constant for approximately 3 months (Cu^{2+} 17 mg $d^{-1}L^{-1}$ and Fe^{3+} 16 mg $d^{-1}L^{-1}$) and maximum concentration was reached after 98 days. The concentrations of both metals remained constant for several weeks after maximum concentration was reached. Current density of Fe^{2+} oxidation was very low for the duration of the experiment (<0.03 mA cm^{-2}) according to which iron existed mostly in Fe^{3+} form.

According to the standard errors of the MLR models and results shown in Table 2, the developed methods are not suitable for analysing low metal ion concentrations (<0.1 g L^{-1}). However, in bioleaching and AMD environments the concentrations of dissolved metal ions are usually high, in the range of 0.1–10 g L^{-1}, and therefore this limitation is not a significant drawback of this technique for these applications. Measurement errors could be reduced by using a rotating disk electrode (RDE), which enhances the mass transfer. For example, Zhang and Yoshihara used cathodic stripping voltammetry on BDD to quantify the concentration of nickel [33] and they found that the sensitivity was significantly improved when mass transfer was

Table 3 Regression statistics, analysis of variance (ANOVA) and coefficients for the MLR model for Cu^{2+} analysis

Regression statistics				
Multiple R				0.9957
R^2				0.9914
Adjusted R^2				0.9909
Standard error				0.0473
Observations				39
ANOVA	df	SS	MS	F
Regression	2	9.28E+00	4.64E + 00	2.08E+03
Residual	36	8.04E−02	2.23E−03	
Total	38	9.36E+00		

Terms	Coefficients	Standard error	t Stat	*P*-value
Intercept	−2.52E−02	1.17E−02	−2.15E+00	3.85E−02
i Fe^{3+} (A cm^{-2}, 10 s)	1.14E+03	5.54E+01	2.06E+01	1.74E−21
i Cu^{3+} (A cm^{-2}, 5 s) * pH	−2.52E+02	3.93E+00	−6.42E+01	9.92E−39

Table 4 Regression statistics, ANOVA and coefficients for the MLR model for Fe^{3+} analysis

Regression statistics				
Multiple R				0.9953
R^2				0.9906
Adjusted R^2				0.9898
Standard error				0.0826
Observations				39
ANOVA	df	SS	MS	F
Regression	3	2.52E+01	8.39E+00	1.23E+03
Residual	35	2.39E−01	6.82E−03	
Total	38	2.54E+01		

Terms	Coefficients	Standard error	t Stat	*P*-value
Intercept	−4.65E−02	2.17E−02	−2.14E+00	3.90E−02
i Fe^{3+} (A cm^{-2}, 10 s)	−1.52E+04	1.01E+03	−1.51E+01	6.72E−17
i Cu^{2+} (A cm^{-2}, 5 s)	−4.55E+02	2.18E+01	−2.09E+01	2.51E−21
i Fe^{3+} (A cm^{-2}, 10 s) * pH	8.76E+03	7.28E+ 02	1.20E+01	5.51E−14

enhanced by using RDE. Jin and Botte were able to reach LOD of 0.02 mM for Fe^{2+} and Fe^{3+} analysis using RDE [32]. However, the aim of this research work was to develop a robust and mechanically simple sensor which could be used on-site and possibly inside bioleaching heaps and therefore RDE was not used.

The analytical methods used in this study may also be improved by employing different surface pretreatments to the BDD electrode. According to literature, pretreatment has a significant effect on the electrochemical properties of BDD [29, 34–36]. Hydrogen-terminated and oxygen-terminated surfaces have different electrical conductivities, wetting properties and chemical reactivities. Termination of the diamond interface can be changed by various procedures including electrochemical methods [34] and plasma treatments [29]. It is possible that electrochemical cycling pretreatment conducted in this research was not optimal for the analysis methods and this requires further investigation.

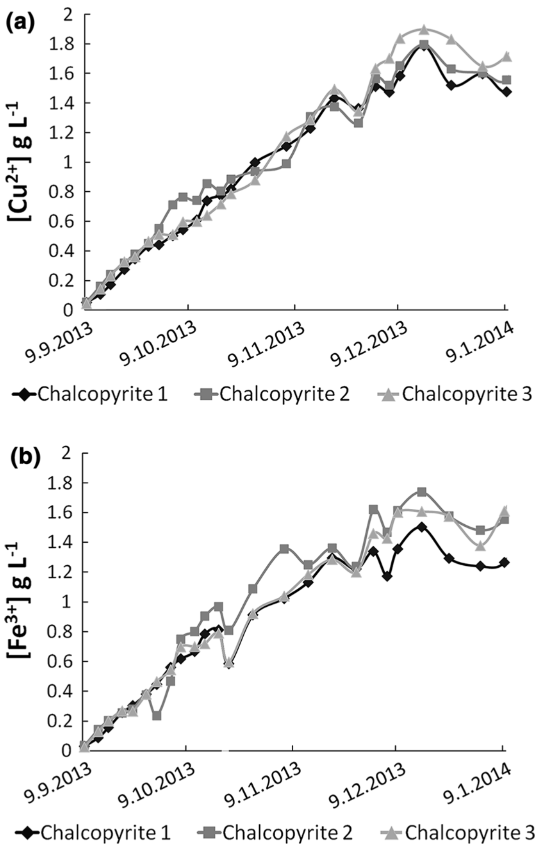

Fig. 8 Monitoring the bioleaching of **a** Cu^{2+} and **b** Fe^{3+} using the developed electroanalytical method and MLR calibration

4 Conclusions

In this research a simple and robust chronoamperometric method for the determination of Cu^{2+}, Fe^{3+} and Fe^{2+} concentrations in acidic solutions was developed. A boron-doped diamond was selected as the electrode material for these analyses because it has a wide potential window and is particularly stable. No interferences caused by other metal ions were observed when Fe^{2+} was analysed. However, reduction of Fe^{3+} took place at the same potential in which Cu^{2+} was measured causing minor interference to the Cu^{2+} measurements. The MLR models developed to quantify Cu^{2+} and Fe^{3+} yielded high coefficients of determination and acceptable standard errors. Variances of the models were primarily explained by the variations in the current signal. This work shows that chronoamperometric methods are suitable for analysing Cu^{2+}, Fe^{3+} and Fe^{2+} in AMD and bioleaching environments. Further optimisation of analysis methods by electrode pre-treatments may reduce the LOD for all three analytes.

Acknowledgments The authors would like to acknowledge the financial support received from the CSIRO Office of the Chief Executive. Discussions with Professor Roger Horn, Dr David Nairn, Mike Horne and Dr Jean-Pierre Veder are appreciated.

References

1. Akcil A, Koldas S (2006) Acid mine drainage (AMD): causes, treatment and case studies. J Clean Prod 14:1139–1145
2. Johnson DB, Hallberg KB (2005) Acid mine drainage remediation options: a review. Sci Total Environ 338:3–14
3. Sheoran AS, Sheoran V (2006) Heavy metal removal mechanism of acid mine drainage in wetlands: a critical review. Minerals Eng 19:105–116
4. Malmqvist B, Hoffsten P (1999) Influence of drainage from old mine deposits on benthic macroinvertebrate communities in central Swedish streams. Water Res 33:2415–2423
5. Sasaki A, Ito A, Aizawa J, Umita T (2005) Influence of water and sediment quality on benthic biota in an acidified river. Water Res 39:2517–2526
6. Hallberg KB (2010) New perspectives in acid mine drainage microbiology. Hydrometallurgy 104:448–453
7. Pradhan N, Nathsarma KC, Srinivasa Rao K, Sukla LB, Mishra BK (2008) Heap bioleaching of chalcopyrite: a review. Minerals Eng 21:355–365
8. Leahy MJ, Schwarz MP (2009) Modelling jarosite precipitation in isothermal chalcopyrite bioleaching columns. Hydrometallurgy 98:181–191
9. Zhang Y, Qin W, Wang J, Zhen S, Yang C, Zhang J, Nai S, Qiu T (2008) Bioleaching of chalcopyrite by pure and mixed culture. Trans Nonferrous Metal Soc 18:1491–1496
10. Zhao X, Wang R, Lu X, Lu J, Li C, Li J (2013) Bioleaching of chalcopyrite by Acidithiobacillus ferrooxidans. Minerals Eng 53:184–192
11. Vilcáez J, Suto K, Inoue C (2008) Bioleaching of chalcopyrite with thermophiles: temperature–pH–ORP dependence. Int J Miner Process 88:37–44
12. Hulanicki A, vel Krawczyk TK (1987) Behaviour of a chalcocite copper ion-selective electrode in solutions of iron(III) ions. Talanta 34:407–410
13. Radić N, Vudrag M (1984) Kinetic determination of iron(III) with a copper(II) selective electrode based on a metal displacement reaction. J Electroanal Chem Interfacial Electrochem 178:321–327
14. Jung H, Yun S, Kwon J, Zheng Y (2012) Role of iron colloids in copper speciation during neutralization in a coastal acid mine drainage, South Korea: insight from voltammetric analyses and surface complexation modeling. J Geochem Explor 112:244–251
15. Honório GG, Azevedo GC, Matos MAC, de Oliveira MAL, Matos RC (2014) Use of boron-doped diamond electrode pre-treated cathodically for the determination of trace metals in honey by differential pulse voltammetry. Food Control 36:42–48
16. Martin HB, Argoitia A, Landau U, Anderson AB, Angus JC (1996) Hydrogen and Oxygen Evolution on Boron Doped Diamond Electrodes. J Electrochem Soc 143:133–136
17. Ramesham R, Rose MF (1997) Electrochemical characterization of doped and undoped CVD diamond deposited by microwave plasma. Diam Relat Mater 6:17–26
18. Ivandini TA, Sato R, Makide Y, Fujishima A, Einaga Y (2004) Electroanalytical application of modified diamond electrodes. Diam Relat Mater 13:2003–2008
19. Einaga Y, Sato R, Olivia H, Shin D, Ivandini TA, Fujishima A (2004) Modified diamond electrodes for electrolysis and electroanalysis applications. Electrochim Acta 49:3989–3995
20. Sonthalia P, McGaw E, Show Y, Swain GM (2004) Metal ion analysis in contaminated water samples using anodic stripping

voltammetry and a nanocrystalline diamond thin-film electrode. Anal Chim Acta 522:35–44

21. Dragoe D, Spătaru N, Kawasaki R, Manivannan A, Spătaru T, Tryk DA, Fujishima A (2006) Detection of trace levels of Pb^{2+} in tap water at boron-doped diamond electrodes with anodic stripping voltammetry. Electrochim Acta 51:2437–2441
22. Salimi A, Alizadeh V, Hallaj R (2006) Amperometric detection of ultra trace amounts of Hg(I) at the surface boron doped diamond electrode modified with iridium oxide. Talanta 68:1610–1616
23. Manivannan A, Kawasaki R, Tryk DA, Fujishima A (2004) Interaction of Pb and Cd during anodic stripping voltammetric analysis at boron-doped diamond electrodes. Electrochim Acta 49:3313–3318
24. Tan SN, Chen M (2012) Early stage adsorption behaviour of Acidithiobacillus ferrooxidans on minerals I: an experimental approach. Hydrometallurgy 119–120:87–94
25. Ni Y, Li S, Kokot S (2011) Simultaneous voltammetric analysis of tetracycline antibiotics in foods. Food Chem 124:1157–1163
26. Turnes G, Cladera A, Gómez E, Estela JM, Cerdà V (1992) Resolution of highly overlapped differential pulse polarographic and anodic stripping voltammetric peaks by multicomponent analysis. J Electroanal Chem 338:49–60
27. Cladera A, Alpízar J, Estela JM, Cerdà V, Catasús M, Lastres E, García L (1997) Resolution of highly overlapping differential pulse anodic stripping voltammetric signals using multicomponent analysis and neural networks. Anal Chim Acta 350:163–169
28. Vazquez-Arenas J, Vázquez G, Meléndez AM, González I (2007) The Effect of the Cu2+/Cu+ Step on Copper Electrocrystallization in Acid Noncomplexing Electrolytes. J Electrochem Soc 154:473–481
29. Couto AB, Santos LCD, Matsushima JT, Baldan MR, Ferreira NG (2011) Hydrogen and oxygen plasma enhancement in the Cu electrodeposition and consolidation processes on BDD electrode applied to nitrate reduction. Appl Surf Sci 257:10141–10146
30. Volov I, Saito T, West AC (2011) Investigation of Copper Plating and Additive Interactions in the Presence of Fe^{3+}/Fe^{2+} Redox Couple. J Electrochem Soc 158:384–389
31. Khouraibchia Y, Moats MS (2010) Evaluation of the Effect of Copper Electrowinning Parameters on Current Efficiency and Energy Consumption Using Surface Response Methodology. ECS Trans 28:295–306
32. Jin X, Botte G (2009) Electrochemical technique to measure Fe(II) and Fe(III) concentrations simultaneously. J Appl Electrochem 39:1709–1717
33. Zhang Y, Yoshihara S (2004) Cathodic stripping voltammetry of nickel on boron-doped diamond. J Electroanal Chem 573:327–331
34. Hoffmann R, Kriele A, Obloh H, Hees J, Wolfer M, Smirnov W, et al. (2010) Electrochemical hydrogen termination of boron-doped diamond. Appl Phys Lett 97:052103,052103-3
35. Szunerits S, Boukherroub R (2008) Different strategies for functionalization of diamond surfaces. J Solid State Electro 12:1205–1218
36. Ribeiro MC, Silva LGd, Sumodjo PTA (2006) The influence of electrochemical pre-treatment of B-doped diamond films on the electrodeposition of Pt. J Brazil Chem Soc 17:667–673